

# Procedural and learning-based generation of coral reef islands

Submission1265

## Abstract

We propose a procedural method for generating single volcanic islands with coral reefs using user sketching from two projections: a top view, which defines the island's shape, and a profile view, which outlines its elevation. These projections, commonly used in geological and remote sensing domains, are complemented by a user-defined wind field, applied as a distortion field to deform the island's shape, mimicking the effects of wind and waves on the long term and enabling finer user control. We then model the growth of coral on the island and its surrounding to construct the reef following biological observations. Based on these inputs, our method generates a height field of the island. Our method is capable of creating a large variety of island models composing a dataset used for training a conditional Generative Adversarial Network (cGAN). By applying data augmentation, the cGAN allows for even greater variety in the generated islands, providing users with higher freedom and intuitive controls over the shape and structure of the final output.

1    **Keywords:** Procedural modeling, Terrain generation, cGAN,  
2    Coral reef, Sketch-based interface

## 3    1. Introduction

4    Simulating the formation of coral reef islands presents significant  
5    challenges due to the complex interplay of geological, environmental,  
6    and biological factors (**Hopley2014**). One major difficulty lies  
7    in capturing the long-term subsidence of volcanic islands, which  
8    occurs over millions of years, while simultaneously modeling the  
9    upward growth of coral reefs that rely on environmental conditions  
10   such as water depth, temperature, and sunlight. This combination of  
11   slow geological processes and dynamic biological growth is chal-  
12   lenging to replicate in a computational model.

13   Additionally, the biological aspects of coral growth are inher-  
14   ently tied to environmental factors. Coral reefs grow only within a  
15   specific range of water depth and sunlight, and their growth patterns  
16   are affected by the health of the reef ecosystem and the availability  
17   of resources. Accurately modeling these biological dependencies in  
18   a procedural system is challenging, as these factors are numerous  
19   and difficult to generalize. Moreover, the scarcity of data available  
20   obstructs the global understanding of these ecosystems. In a recent  
21   high-resolution mapping of shallow coral reefs (**Lyons2024**), re-  
22   searchers estimated the total surface area of this biome to cover less  
23   than 0.7% of Earth's area, and more specifically that coral habitat  
24   represents less than 0.2%.

25   Moreover, the need to design plausible reef structures in digital  
26   environments for applications such as scientific visualization, sim-  
27   ulation, or digital entertainment, calls for models that balance real-  
28   ism with controllability. Existing terrain generation methods, such  
29   as Perlin noise-based algorithms or uplift-erosion models, are of-  
30   ten ill-suited for these processes. While they can generate natural-

31   looking landscapes (such as alpine landscape, representing about  
32   a quarter of land area (**Korner2014**)), they do not account for the  
33   unique geological and biological interactions that govern coral reef  
34   island formation, thus missing coherency. Capturing these dynam-  
35   ics, while also providing user control during the modeling of a ter-  
36   rain, requires a balance between realism and flexibility, allowing  
37   for both accurate computationally expensive simulation of natural  
38   processes and intuitive user control in interactive time.

39   Despite advances in terrain generation, existing methods strug-  
40   gle with user-controlled design of specific island shapes and achiev-  
41   ing realism without real data. Coral reef islands exemplify this gap:  
42   we lack datasets to directly train deep models, and purely procedur-  
43   al methods require expert tuning to mimic their features.

44   To address these issues, we propose to use curve-based mod-  
45   eling techniques as an initial step in our approach as a means to  
46   efficiently create a large and diverse set of training examples for  
47   a learning-based model. Each synthetic example is represented by  
48   a terrain height field and a corresponding semantic label map that  
49   marks different regions, providing structured input-output pairs for  
50   the learning stage.

51   We trained a conditional Generative Adversarial Network  
52   (cGAN) as the core of our learning-based approach (**Mirza2014;**  
53   **Isola2017**). A cGAN is a type of deep learning model that learns  
54   to generate realistic data based on an input condition or context.  
55   In our case, the cGAN takes as input the semantic label map of  
56   an island generated by the procedural step and learns to produce  
57   a realistic island height field that matches this layout. By training  
58   on a large variety of examples from our curve-based algorithm, the  
59   cGAN captures the subtle terrain features and variations character-  
60   istic of coral reef islands, this approach surpasses the capabilities of  
61   traditional procedural rules, aided by extensive data augmentation.  
62   The cGAN model can be used on its own to generate new island

63 terrains with simplified and more intuitive user inputs through digital drawing, and the model will generate a realistic island terrain  
 64 accordingly.  
 65

66 The key contributions are as follows: 1) a novel curve-based procedural algorithm for shaping island terrains from top and profile views, 2) The training of a deep learning model on synthetic data derived from procedural rules, serving as an abstraction layer that hides underlying complexity, 3) A demonstration that the cGAN approach tolerates imprecise, low-detail user input sketches, broadening usability, without the need for cutting-edge network architectures, and 4) An insight that procedural generation remains essential to produce training data in data-sparse domains such as coral reef islands. These contributions collectively show a pathway to blend user-driven design with learning-based generation in terrain modeling.

## 78 2. Related work

79 Procedural terrain generation spans a spectrum from purely noise-driven algorithms to physics-based simulations and, more recently, data-driven methods. In the context of coral reef islands, where both long-term geological subsidence and biogenic reef accretion interplay, existing approaches fall short in one of two ways: either they lack ecological or geological grounding, or they offer insufficient authoring control.

80 **Procedural and simulation-based methods** Noise-based techniques such as Perlin noise (**Perlin1985**), Simplex noise (**Perlin2001**), and the Diamond-Square algorithm (**Fournier1982**) (often extended via fBm or multifractal noise (**Musgrave1989; Ebert2003**)) remain popular for their simplicity and speed. Island shapes are generated by modulating noise with radial falloff masks (**Olsen2004**), but these methods cannot reproduce reef rings, lagoons, or atoll structures in a geologically coherent manner. They treat terrain purely as a signal-processing problem, separated from processes like volcanic subsidence or coral growth (**Smelik2009; Galin2019**).

81 Simulation-based approaches introduce causality by modeling erosion (**Benes2006; Neidhold2005; Mei2007**), tectonic uplift (**Cordonnier2016; Cordonnier2017a; Schott2023**), or vegetation-terrain feedback (**Ecormier-Nocca2021; Cordonnier2017b**). Hydraulic and thermal erosion capture fluvial networks and slope-driven mass wasting, but they omit underwater sedimentation and biogenic carbonate accretion. Tectonic and isostatic models excel at orogeny but ignore coral reef dynamics, while vegetation-based methods do not generalize to marine ecosystems. Consequently, none of these simulations jointly capture the slow subsidence of volcanic islands and the compensatory growth of surrounding reefs on the timescales required for atoll formation.

82 **Sketch-based terrain modeling** Sketch-driven interfaces bridge user intent and procedural detail. Curve-based systems let users draw ridges, valleys, or coastlines that guide surface deformation and noise propagation (**Gain2009; Hnaidi2010**). Constraint-based methods extend this by enforcing absolute elevation or slope values at control curves or points, solved via diffusion or fractal interpolation (**Gasch2020; Talgorn2018**), and even gradient-domain

117 editing for slope control (**Guerin2022**). Semantic approaches encode high-level "terrain atoms" from a dictionary of primitives  
 118 (**Genevaux2015**) or interpret geological schematics into 3D models  
 119 (**Natali2012**). While these techniques grant artists fine-grained  
 120 control, they typically lack ecological constraints and have not been  
 121 tailored to marine biogeomorphology.  
 122

123 **Learning-based terrain synthesis** Deep generative models offer  
 124 a way to learn complex patterns without explicit procedural rules.  
 125 Unconditional GANs have been applied to digital elevation maps of  
 126 mountains (**WulffJensen2018**) and joint height-texture synthesis  
 127 (**Spick2019**), but their reliance on latent noise prevents precise lay-  
 128 out control. Two-stage pipelines use an initial GAN for heightmaps  
 129 and a conditional GAN for textures (**Beckham2017**) or reverse the  
 130 order (imagery-to-DEM) (**Panagiotou2020**), yet still lack the abil-  
 131 ity to guide authoring.

132 Conditional GANs (cGANs) extend image-to-image translation  
 133 methods such as pix2pix (**Isola2017**) to terrain, enabling sketch- or  
 134 label-map-conditioned generation. Prior work includes sketch-to-  
 135 DEM translation for generic landforms (**Guerin2017**) and sparse  
 136 "altitude dot" conditioning (**Voulgaris2021**), as well as cGANs  
 137 that invert satellite imagery into elevation (**Sisodia2022**). However,  
 138 these models require extensive paired real-world datasets which are  
 139 scarce for coral reef islands.

## 140 3. Overview

141 Our method for procedural generation of coral reef islands is com-  
 142 posed of two independent modeling techniques shown in Figure 1.  
 143 A first algorithm, curve-based (top-left blue block, is presented in  
 144 Section 4), parametrize the surface of islands by a top-view sketch  
 145 interface, describing the outlines of the regions composing it and a  
 146 stroke-based wind field deforming them, as well as a profile-view  
 147 sketch describing for each region its altitude and resistance to de-  
 148 formations. User inputs are given as 1D functions (altitude and re-  
 149 sistance), a 1D polar function (island outlines) and a 2D vector field  
 150 (wind field) as shown in Figure 2, which are convient to randomize  
 151 through the use of noise, but hindering users' modeling freedom.

152 On the other hand, we include a second generation algorithm,  
 153 learning-based (right red blocks from the pipeline figure, developed  
 154 in Section 6), which train a neural generator  $G$  to transform a la-  
 155 beled image into a height field. Paralelly, a discriminator  $D$  is train  
 156 to distinguish height fields provided from the training set against  
 157 height fields generated by  $G$ . This adversarial training strengthen  
 158 the outputs of the generator, up to the point where we discard the  
 159 discriminator and training data, only keeping the generation step  
 160 (bottom-right). Users are then able to provide unseen label maps  
 161 and obtain height fields as close as possible to the training dataset.  
 162 This method for terrain modeling is poorly constraint, however re-  
 163 quires a large amount of prior data in its training set, which are not  
 164 available in our case.

165 We connect these two algorithms through a process of dataset  
 166 generation (central orange block, described in Section 5) in order to  
 167 enforce the benefits of each while reducing their limitations. Given  
 168 the initial curve-based user inputs, we create a dataset composed of  
 169 similar samples processed by our first algorithm, rasterized into a  
 170 2D image of the parametrized regions, and paired with the resulting

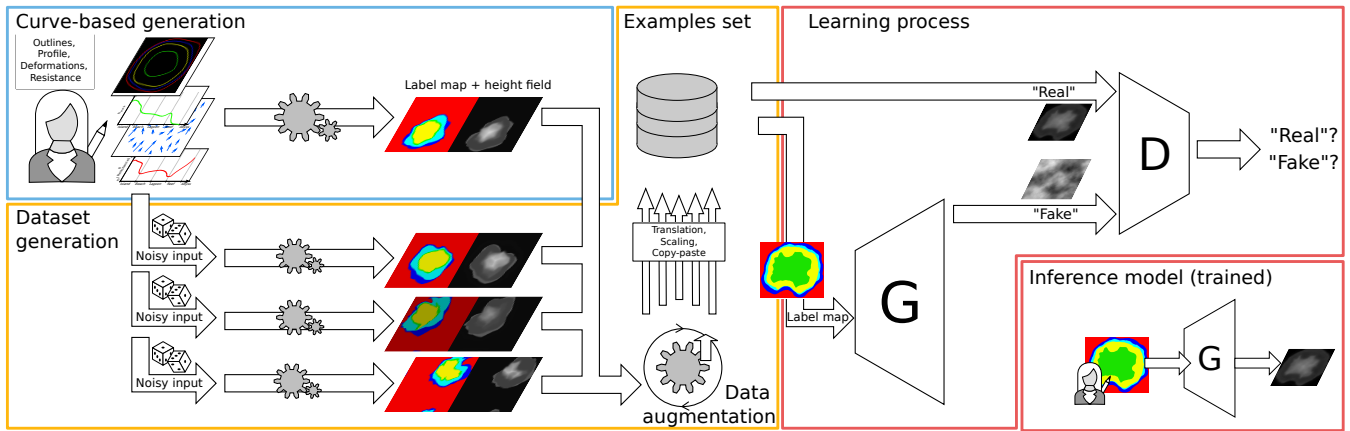


**Figure 1:** Our pipeline first prompt our user to create single pairs of coral reef islands' height fields and label maps using our proposed curve-based modeling algorithm (Section 4). The same algorithm is applied multiple times on randomly altered versions of the user input to create a dataset, which we further enhance with data augmentation techniques Section 5. Finally, we train a conditional Generative Adversarial Network which can then be used standalone to create height fields from labeled sketches (Section 6).

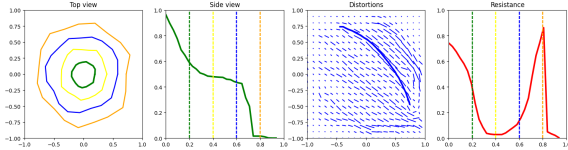


**Figure 2:** The user can interact directly on the island by editing the different canvases in no specific order. This UI shows, from left to right, the top-view sketch with the different outlines of each regions, the profile-view sketch with the outlines represented in dotted lines, the wind velocity sketch drawn with strokes (last stroke is visible), and the resistance function showing here a high resistance at the top of the island and on the front reef.

height field. We then enhance greatly the size of the dataset by employing various data augmentation techniques such as translations, scaling and copy-pasting of multiple islands in a single sample. We then obtain a dataset large enough for training our cGAN and enable the modeler to create procedurally coral reef islands with a high level of control.

#### 4. Curve-based island generation

The generation of coral reef island terrains involves a structured process that takes the user's sketches and produces a complete 3D terrain model. This process begins with the creation of the initial height field based on the user's input, followed by the application of wind deformation to introduce natural variations, and concludes with the integration of coral reef features through subsidence and coral growth modeling.

The generation of coral reef islands in this system begins with two intuitive sketch-based inputs from the user: a top-view sketch and a profile-view sketch, which define the islands horizontal lay-

out and vertical elevation profile. In addition to these sketches, the user can further refine the terrain by applying wind deformation strokes, which simulate the effects of wind and waves on the islands shape. This combination of sketches and wind inputs gives users precise control over both the islands structure and its natural variations, such as irregular coastlines or concave features. We will present the usefulness of these sketches in this section, and describe the technical details in the next section.

#### 4.1. Initial height field generation

The top-view sketch defines the island's outline as seen from above. Using a simple drawing interface, the user delineates concentric boundaries for key regions such as the island itself, the beaches, the lagoon, and the surrounding abyss, around the canvas center. Each boundary is represented in polar coordinates, where  $r_p$  is the radial distance from the island's center and  $\theta_p$  is the angular position. Allowing  $r$  to vary with  $\theta$  introduces irregular, natural shapes rather than perfect circles (Figure 3).

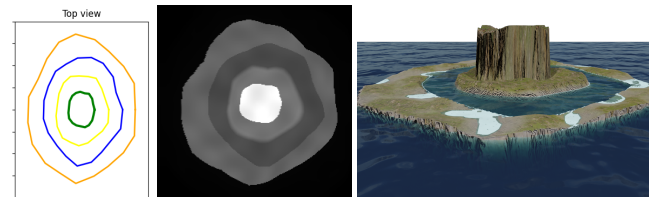


**Figure 3:** Using only the outlines from the top-view sketch, each point in the field is assigned a region (island, beach, lagoon, abyss), which later guides its height assignment.

The profile-view sketch defines the island's vertical elevation

206 along any radial direction. Here, the user draws a curve that  
 207 specifies height at key terrain milestones, such as the central peak, island  
 208 border, beach, lagoon, and abyss, creating a continuous 1D height  
 209 function  $h_{\text{profile}}(\tilde{x})$  where  $\tilde{x}$  is a parametric distance measuring position  
 210 along the sequence of regions. This continuous profile ensures  
 211 smooth elevation transitions across all terrain features.

212 By combining the top-view and profile-  
 213 view sketches via revolution modeling, the  
 214 system generates a full 3D terrain model that  
 215 matches the user's design. The process begins  
 216 by transforming those two sketches into  
 217 a coherent height field (Figure 5).

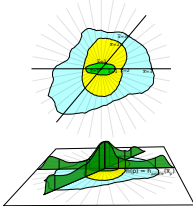


**Figure 4:** Parametric distance  $\tilde{x}$  depending on angle  $\theta$ .

218 For any point  $\mathbf{p}$  on the terrain, the system  
 219 computes polar coordinates  $(r_{\mathbf{p}}, \theta_{\mathbf{p}})$ . The radial  
 220 distance  $r_{\mathbf{p}}$  determines which region  
 221 the point belongs to (island, beach, lagoon,  
 222 reef, or abyss) based on the user-defined ra-  
 223 dial limits. Those outlines from the top-view  
 224 sketch provide the exact boundaries between  
 225 regions.

226 Each point's height is computed using the  
 227 profile function  $h_{\text{profile}}(\tilde{x})$ . Instead of using  
 228 the raw radial distance  $r_{\mathbf{p}}$ , we define a parametric region distance  $\tilde{x}_{\mathbf{p}}$   
 229 that maps each point to a normalized position along the concentric  
 230 regions (see Figure 4). The radial space is divided by user-defined  
 231 boundaries  $R_0, R_1, \dots, R_n$ , corresponding to the island center, bor-  
 232 der, beach, lagoon, and abyss.

233 When a point  $\mathbf{p}$  lies between two boundaries, say  $R_i$  and  $R_{i+1}$ ,  
 234 its parametric distance is

$$\tilde{x}_{\mathbf{p}} = i + \frac{r_{\mathbf{p}} - R_i}{R_{i+1} - R_i}, \quad (1)$$

235 where  $i$  is the index of the region containing  $\mathbf{p}$  (i.e.,  $R_i \leq r_{\mathbf{p}} < R_{i+1}$ ). This linear mapping stretches each region's radial span to  
 236 the interval  $[i, i+1]$ , ensuring smooth interpolation across region  
 237 boundaries. The final height at point  $\mathbf{p}$  is then  
 238

$$h(\mathbf{p}) = h_{\text{profile}}(\tilde{x}_{\mathbf{p}}). \quad (2)$$

#### 239 4.1.1. Wind deformation

240 To break the radial symmetry inherent in sketch-based terrain gen-  
 241 eration and introduce more organic island shapes, we allow the user  
 242 to define a wind velocity field via freehand strokes on a 2D canvas.  
 243 Each stroke is represented as a parametric curve  $C$ , interpreted as a  
 244 local wind flow with direction  $C'$ , strength  $S$ , and influence width  
 245  $\sigma$ . These strokes simulate wind and wave erosion effects on the  
 246 terrain.

247 The deformation vector at any terrain point  $\mathbf{p}$  is computed as a  
 248 sum over all strokes, weighted by a Gaussian falloff centered on the  
 249 closest point  $\mathbf{p}_C^*$  along each curve (Figure 6, top):

$$\Phi(\mathbf{p}) = \sum_{C \in \text{curves}} S \frac{C'(\mathbf{q})}{\|C'(\mathbf{q})\|} \cdot G_{\sigma}(\|\mathbf{p} - \mathbf{p}_C^*\|) \quad (3)$$

$$G_{\sigma}(x) = \frac{1}{\sigma\sqrt{2\pi}} e^{-\frac{x^2}{2\sigma^2}}. \quad (4)$$

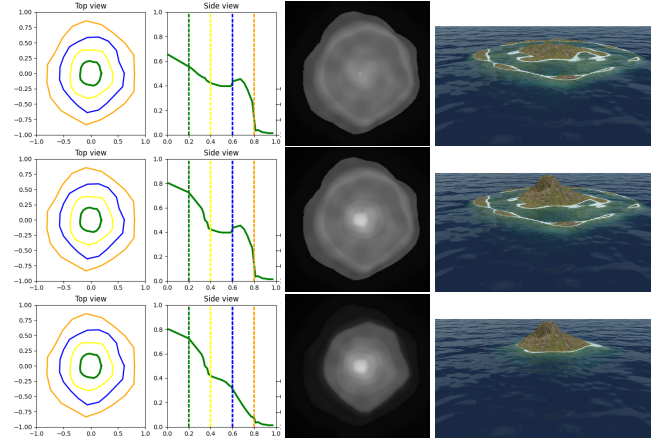


**Figure 5:** Providing a smooth function between each region results in islands with plausible reliefs. We fixed the outlines while editing only the height function in order to produce, from top to bottom, a low island, a coral reef island, and finally an identical island without the reef.

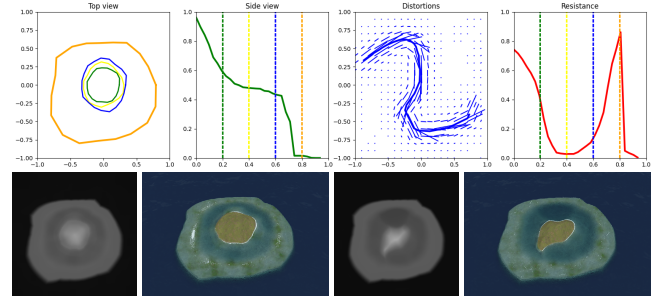


**Figure 6:** Defining a top-view wind vector field from user-provided strokes (top, blue) in association with a resistance function (top, red), a height field is deformed accordingly. Right: original height field and render; Left: altered results. The beach and lagoon regions are defined with low resistance, which is visible by having only these regions deformed in bottom results.

250 To preserve semantic structure across terrain regions, a resis-  
 251 tance function  $\rho(\tilde{x})$  modulates the deformation based on terrain  
 252 zones such as beach, lagoon, or abyss (Figure 7). The final defor-  
 253 mation vector becomes:

$$\tilde{\Phi}(\mathbf{p}) = (1 - \rho(\tilde{x}_{\mathbf{p}})) \cdot \Phi(\mathbf{p}). \quad (5)$$

254 This warp is applied to both the height field and the label map,  
 255 ensuring consistent semantic deformation. For example, applying  
 256 strokes to one side of a circular island creates concave coastlines  
 257 while leaving high-resistance regions (e.g., the abyss) unaffected,  
 258 simulating the localized impact of natural erosion (Figure 6, bot-  
 259 tom).

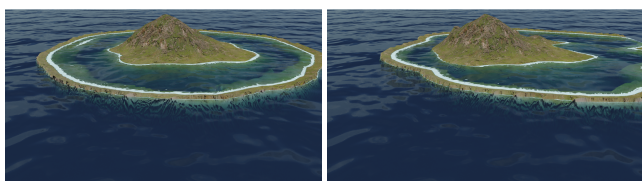


**Figure 7:** (Left) An island defined with a high resistance, under a uniform lateral wind velocity field, and (right) the same island with lower resistance on the reef borders, simulating the effect of coastal erosion.

## 260 4.2. Coral reef modeling

261 Once the terrain has been generated and deformed by the wind, we  
262 simulate the long-term geological evolution of coral reef islands  
263 through two parallel processes: the subsidence of the volcanic is-  
264 land and the upward growth of coral reefs. As observed in nature,  
265 the volcanic base sinks over time while coral formations grow ver-  
266 tically to remain close to the water surface, following the "keep-up"  
267 strategy of reef development.

### 268 4.2.1. Subsidence

269 Subsidence is modeled by uniformly scaling the original terrain  
270 height downward, simulating the gradual sinking of the volcanic  
271 landmass due to tectonic processes. The user specifies a subsidence  
272 rate  $\lambda \in [0, 1]$ , which controls how much the island has sunk. The  
273 subsided terrain is computed as:

$$274 h_{\text{subsid}}(\mathbf{p}) = (1 - \lambda) \cdot h_0(\mathbf{p}) \quad (6)$$

275 This factor is applied uniformly across the island, offering a geo-  
276 logically plausible and computationally efficient approximation of  
277 large-scale subsidence.

### 278 4.2.2. Coral reef growth

279 Coral reef growth is modeled independently from the subsiding ter-  
280 rain. The system generates a coral-specific height field  $h_{\text{coral}}(\mathbf{p})$   
281 that remains near the sea surface regardless of the island's verti-  
282 cal shift, reflecting coral growth in biologically viable depth ranges  
283 (typically 0-30 meters below sea level).

284 We define distinct reef zones anchored at specific depths:

- 285 • Reef crest near sea level:  $h_{\text{crest}} = -2 \text{ m}$
- 286 • Back reef and lagoon:  $h_{\text{back}} = -20 \text{ m}$
- 287 • Fore reef sloping to abyss:  $h_{\text{abyss}} = -100 \text{ m}$

288 Each reef subregion is defined over a parametric domain  $x \in$   
289  $[0, 1]$ , with  $x = 0$  the beginning of the reef region and  $x = 1$  its end,  
290 directly inputting the parametric distance  $x = \tilde{x} - i_{\text{reef region}}$ . For in-  
291 stance:

- 292 • Back reef:  $x_{\text{back,start}} = 0, x_{\text{back,end}} = 0.5$

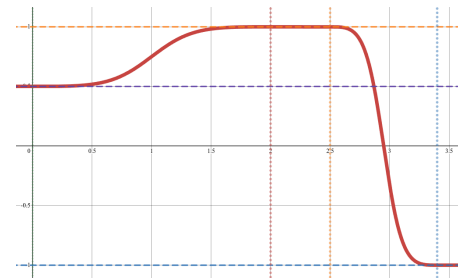


**Figure 8:** The modeling of the reef growth in our model is described by a piecewise function  $h_{\text{coral}}$  which is flat in the lagoon, the crest and abyss, and follows a smoothstep function as transitions for the backreef and fore reef regions. Zones' anchor heights are represented by horizontal dashed lines; zones' limits are dotted vertical lines.

- 292 • Reef crest:  $x_{\text{crest,start}} = 0.75, x_{\text{crest,end}} = 0.8$
- 293 • Abyss begins at  $x_{\text{abyss,start}} = 1$

294 We model transition zones between these regions using a  
295 smoothstep operator:

$$296 \text{smoothstep}(x) = 3x^2 - 2x^3 \quad (7)$$

297 We denote the interpolating function as:

$$298 S(a, b, x_0, x_1, x) = a + (b - a) \text{smoothstep}\left(\frac{x - x_0}{x_1 - x_0}\right) \quad (8)$$

299 The complete coral height field, as displayed in Figure 8, is built  
300 as a piecewise function:

$$301 h_{\text{coral}}(x) = \sum_{r \in \text{subregions}} \begin{cases} h_r & \text{if } x_{r,\text{start}} \leq x \leq x_{r,\text{end}} \\ 0 & \text{otherwise} \end{cases} \\ 302 + \sum_{t \in \text{transitions}} \begin{cases} S(h_t, h_{t+1}, x_{t,\text{end}}, x_{t+1,\text{start}}, x) & \text{if } x_{t,\text{end}} < x < x_{t+1,\text{start}} \\ 0 & \text{otherwise} \end{cases} \quad (9)$$

### 4.2.3. Output

303 Finally, we merge the island base height field and the coral reef  
304 height field by our *ad-hoc* smooth maximum operator  $\text{smax}$  defined  
305 as:

$$306 \text{smax}(a, b) = \begin{cases} a + \frac{\delta}{2k} \left( \frac{1}{1 + e^{-k\delta}} + \frac{1}{1 - e^{-k\delta}} \right) & \text{for } a \neq b \\ a + \frac{1}{2k} & \text{for } a = b \end{cases} \quad (10)$$

307 with  $\delta = b - a$  for conciseness, and  $k$  a sharpness parameter approx-  
308 imating the max operator as  $k$  grows. At  $k = 5$ , the operator  $\text{max}$  is  
309 already well approximated while conserving continuousness in the  
310 resulting height field  $\mathcal{H}(p) = \text{smax}(h_{\text{subsid}}(\mathbf{p}), h_{\text{coral}}(\mathbf{p}))$ .

311 The resulting terrain represents a plausible coral reef island,  
312 where the volcanic island has subsided, and coral reefs have grown

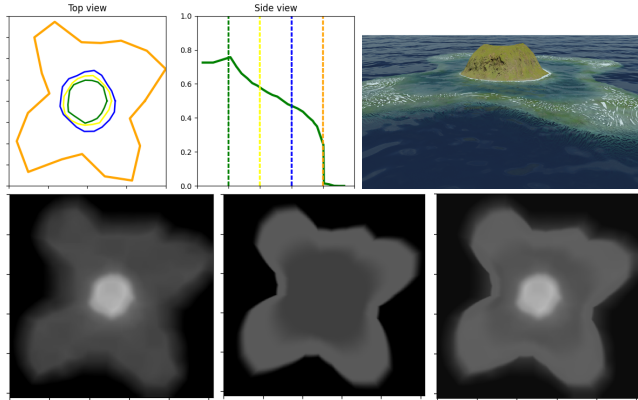


**Figure 9:** Volcano with single vent. (Bottom right) The initial height field is computed directly from the user input, (bottom center) the reef height field is outputed from Equation (9), and finally, (bottom left) we blend the two results with Equation (10).

upward to keep pace with the water level (Figure 9). The smooth blending between the subsided terrain and the coral features ensures a natural transition between regions like the island, lagoon, and coral reefs.

## 5. Data generation

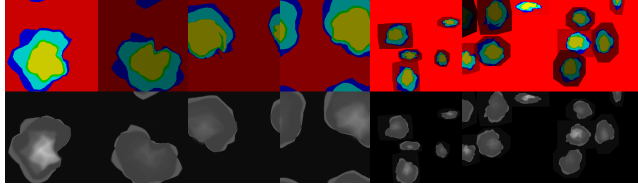


**Figure 10:** Examples from a dataset with increasing data augmentation.

The creation of the dataset is done through the use of the procedural curve-based modeling algorithm for which we alter the input parameters.

For each generation, the top-view and profile-view sketches use an initial layout. Each outline of the top-view sketch is defined as a centered circle of random radius  $r_{\min} \leq r^* \leq r_{\max}$ . We add another deformation based on fBm noise  $\eta$  such that the final contour, profile, and resistances, are defined as

$$\begin{aligned} r(\theta) &= r^* + \eta_{\text{contours}}(\theta) \\ h_{\text{profile}}(\tilde{x}) &= h_{\text{profile}}^*(\tilde{x}) \cdot \eta_{\text{profile}}(\tilde{x}) \\ \rho(\tilde{x}) &= \rho^*(\tilde{x}) \cdot \eta_{\text{resistance}}(\tilde{x}) \end{aligned}$$

Finally, we need to generate a random wind field. The realistic nature of wind is ignored for the generation of the wind strokes in order to provide complexity and variety in the results. We generate

a random number  $n$  of strokes and their path by a uniformly sampling a random number  $m$  of points. The spread and intensity of each stroke is also random.

Once all inputs are set, we generate an example for multiple level of subsidence  $\lambda \in [0, 1]$  to obtain a height field incorporating the coral reef modeling and the associated label map.

We use of the Hue component to encode the labels directly from the parametric distance  $H = [\tilde{x}]$  while the subsidence rate into the Value component  $V = \lambda$ . Moreover, we purposefully left the Saturation component unchanged at this stage, reserving space for potentially including another parameter in the future.

## Data augmentation

To enhance the variety of the dataset and improve the model's ability to generalize, we apply several data augmentation techniques in addition of the usual affine transformations (rotation, scaling, and flipping):

*Translation:* Since the original algorithm always centers the island, we translate the islands within the image to remove this constraint (Figure 10, leftmost). This ensures that the cGAN can generate islands in any position within the frame. By wrapping the island on the borders, the model learns that data can appear on the edges on the image.

*Copy-paste:* In some cases, we combine multiple islands into a single sample, with only a maximum intersection over union (IoU) of 10%, allowing the abysses to overlap but without obtaining other region types to merge. Height fields blending is done through the smooth maximum function from Equation (10), and the label blending uses the usual max operator. The regions not covered by any island are assigned the abyss ID, which is very close to the minimal height, meaning that in this case specifically, the subsidence factor (Value channel) is close to irrelevant (Figure 10, rightmost).

All augmentation techniques are applied both to the height field and the label map simultaneously to ensure consistency between the input (the label map) and the output (the height field).

## 6. Learning-based generation

In this section, we introduce the use of a conditional Generative Adversarial Network (cGAN), specifically the pix2pix model proposed by **Isola2017**, to enhance the island generation process by increasing the variety and flexibility of terrains. While the curve-based modeling algorithm can create numerous island examples, cGAN provides additional flexibility in generating more complex terrain without the rigid constraints of the curve-based algorithm that stem from our initial assumptions based on coral reef formation theory.

The training was performed using a batch size of 1, and optimized using the Adam optimizer with a learning rate of 0.0002 and momentum parameters  $\beta_1 = 0.5$  and  $\beta_2 = 0.999$ . The loss function combined a conditional adversarial loss and an L1 loss, where the L1 loss was weighted by a factor  $\lambda = 100$ . The generator follows

375 a U-Net architecture with encoder-decoder layers and skip connections,  
 376 while the discriminator was based on a PatchGAN, classifying  
 377 local image patches. These parameters are directly used from  
 378 the original paper.

379 The inference of our model, with a dataset of approximatively  
 380 10 000 examples representing about 30 minutes of training, still  
 381 outputs grid artifacts, visible in Figure 11. After the second epoch,  
 382 visual artifacts are already rare. This training time seems long but,  
 383 at the best of our knowledge, is the shortest training time for terrain  
 384 generation with learning-based approach in the litterature, mostly  
 385 due to the mathematical nature of our dataset.

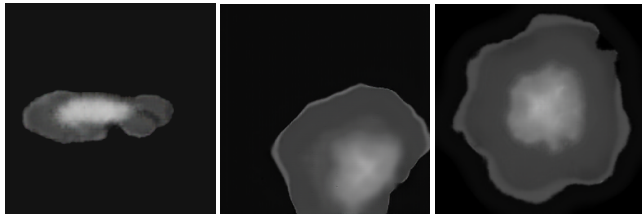


**Figure 11:** After the first epoch (left), grid artifacts similar to low resolution image are visible, but are being corrected during a second epoch (middle). After the second epoch, erosion patterns appear in the hieght fields (right).

386 The Python script for the initial island dataset generation is  
 387 poorly optimized and takes about 2.5s per island of size  $256 \times 256$   
 388 as the parallelization does not take place here. Implementing an op-  
 389 timized C++ version of the initial generation process reduces this  
 390 execution time to 50ms per generation.

391 On the other hand, the inference time of our deep learning model  
 392 for a single input image of dimension  $256 \times 256$  is constant what-  
 393 ever the complexity of the scene. Using the NVIDIA GeForce GTX  
 394 1650 Ti GPU with Python 3.10 and PyTorch version 2.5.1+cu121,  
 395 the inference time measured is 5ms (std 1.1ms).

## 396 7. Results

397 The resulting model for coral island generation enables a high  
 398 control-level from a user perspective as the unconstraint painting  
 399 allows for complex scenarios while producing in real-time the re-  
 400 sulting height fields. In this chapter we used the software Blender  
 401 to provide renders directly from the outputted height fields. As our  
 402 pix2pix model is trained to output  $256 \times 256$  images, the resolution  
 403 of the 3D models is limited by this architecture.

404 Using deep-learning-based models, most constraints from our  
 405 initial assumptions are lifted (radial layout, isolated islands, ...).  
 406 The control over the overall shapes of the islands regions are given  
 407 through digital painting, here using the GIMP software. Each pixel  
 408 of the image are encoded in HSV, with the region identifier encoded  
 409 in the Hue channel. The user may increase or decrease the subsi-  
 410 dence level of the island by modifying the Saturation channel over  
 411 the whole image (see Figure 12).

412 Since the model is based on statistics over the pixel values in-  
 413 stead of hard values, users are not limited to a finite number of

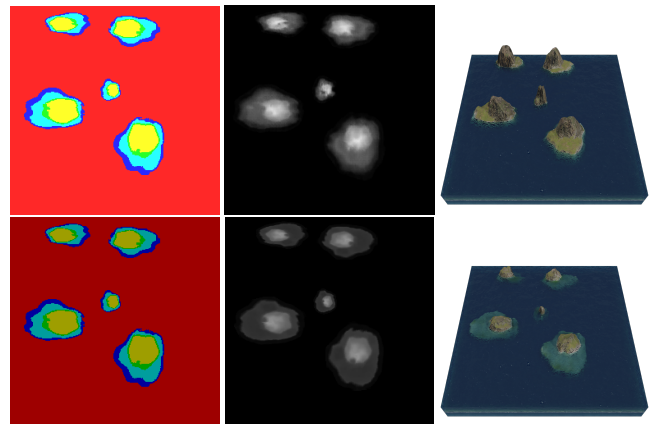


**Figure 12:** An identical label map yield similar height fields over multiple inferences from the model, even after modifying the subsidence factor (visible in the luminosity of the input image).

414 region identifiers, meaning that the output is more or less robust to  
 415 noise (due to image compression, for example) and to the fuzzy val-  
 416 ues resulting from anti-aliasing of brushes often set by default, or  
 417 resizing algorithm, by image editors, or even due to compression  
 418 algorithm. The example displayed in Figure 13 presents a sketch  
 419 for which the outlines of the regions are at the same time blurry  
 420 and with layouts that are not expected (such as the small red re-  
 421 gions inside the southern lagoon region or the adjacency of beach  
 422 regions directly with the abyssal region) on the top figure and over-  
 423 saturated on the bottom figure. The learned model does not include  
 424 inconsistancies and results in plausible 3D models. We can note  
 425 that the input label map doesn't require to be hand drawn, as a sim-  
 426 ple Perlin noise can produce it randomly, as shown in the examples  
 427 of Figure 16.

428 The tolerance over the input values may be used to provide even  
 429 more control about the transitions between two regions. Figure 14  
 430 shows an example of input map with regions that are leaking over  
 431 neighboring regions, and the introduction of new hue values non-  
 432 existant in the dataset (light green and dark green) but are the inter-  
 433 polated hue value of mountain regions and beach regions.

434 Since the curve-based procedural phase included low random-  
 435 ness, the output of the cGAN is limiting its unpredictability and the  
 436 results to a slight change on the input create only slight changes on  
 437 the output, preventing unexpected results. Figure 12 shows the re-  
 438 sult of an input map with only a variation on the subsidence level,  
 439 the resulting height fields are very similar. Adding the real-time  
 440 computation of outputs, it becomes possible to construct progres-  
 441 sively a landscape and correct small mistakes to intuitively design  
 442 islands inspired by real-world regions. A creation of an island simi-  
 443 lar to Mayotte, presented in Figure 15 was hand-made in few min-  
 444 utes.

**Limitations** While this approach brings significant advantages,  
 there are also some limitations to consider. The reliance on a syn-  
 synthetic dataset means that the cGAN inherits some biases and lim-  
 itations of our or initial curve-based algorithm. This could limit

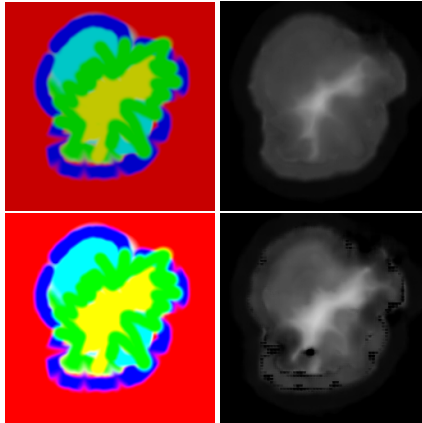


**Figure 13:** User applied fuzzy brushes to draw the label map, resulting in some pixels that are inconsistent with the dataset and unlogical island layouts: abyss regions (red) are found between beach (green), lagoon (cyan) and reef regions (blue). The neural model ignores the layout inconsistencies, and partially over-saturation as long as the pixel isn't completely white.

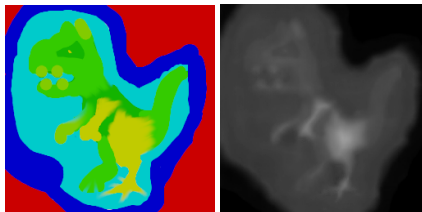


**Figure 14:** Without constraints on the generation, the user may use unrealistic layout and the neural network will however output a plausible result. Here new colors has been added (pistachio), but the network naturally consider it as a transition from mountain to beach.

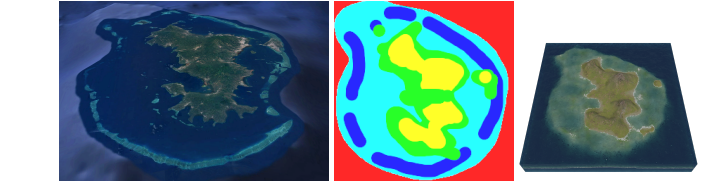


**Figure 15:** Comparison between of real (left, from Google Earth) and synthetic (right) islands of Mayotte. The label map (center) is hand drawn to match approximatively its real-world counterpart.

466 of cGANs (**Park2019**), or models with style transfer functionalities  
 467 (**Gatys2015; Zhu2020**) in order to change the overall aspect  
 468 of a terrain (**Perche2023a; Perche2023b**), use text-to-images models  
 469 (**Rombach2021; Radford2021**) to generate height fields from a  
 470 verbal prompt, or super-resolution models (**Dong2014**) to increase  
 471 the definition of details in the final output (**Guerin2016a**).

## 472 8. Conclusion and future work

473 This work has presented a novel approach to generating coral reef  
 474 island terrains by combining traditional procedural methods with  
 475 deep learning techniques. We first developed a procedural genera-  
 476 tion algorithm capable of creating a wide variety of island terrains  
 477 through a combination of top-view and profile-view sketches, wind  
 478 deformation, and subsidence and coral reef growth simulation. By  
 479 applying these methods, we were able to produce realistic terrains  
 480 based on geological processes, capturing key features of coral reef  
 481 islands such as beaches, lagoons, and coral reefs.

482 To further enhance flexibility and realism in the generation pro-  
 483 cess, we incorporated a conditional Generative Adversarial Net-  
 484 work (cGAN), using the pix2pix model to generate height maps  
 485 from label maps of island features. The cGAN model allowed us to  
 486 overcome some of the constraints inherent in the procedural algo-  
 487 rithm, such as radial symmetry and fixed island positioning. With  
 488 data augmentation techniques, we were able to train the cGAN on  
 489 a synthetic dataset, generating varied and realistic island terrains.

449 the true diversity of the terrains that the model can generate, as the  
 450 output is confined by the patterns present in the training data. Addi-  
 451 tionally, the cGAN model's internal logic lacks transparency, offer-  
 452 ing limited user control over the generation process once the model  
 453 has been trained. Moreover the training time is far from real-time.

454 **Future work** Further improvements could be made to the syn-  
 455 synthetic dataset. Incorporating more complex geological processes,  
 456 such as wave erosion or tidal influences, could lead to even more  
 457 realistic terrains. Additionally, refining the way islands are blended  
 458 in multi-island samples, or adding more diverse input conditions  
 459 (e.g., different geological settings), could help the model general-  
 460 ize better and produce more varied and dynamic landscapes. While  
 461 the current model allows for rapid terrain generation, adding more  
 462 options for users to interact with the cGAN, such as tweaking pa-  
 463 rameters like wind strength or island size, could enhance the flex-  
 464 ibility of the system. Many other neural networks models could  
 465 be exploited to increase the possibilities, such as newer variants

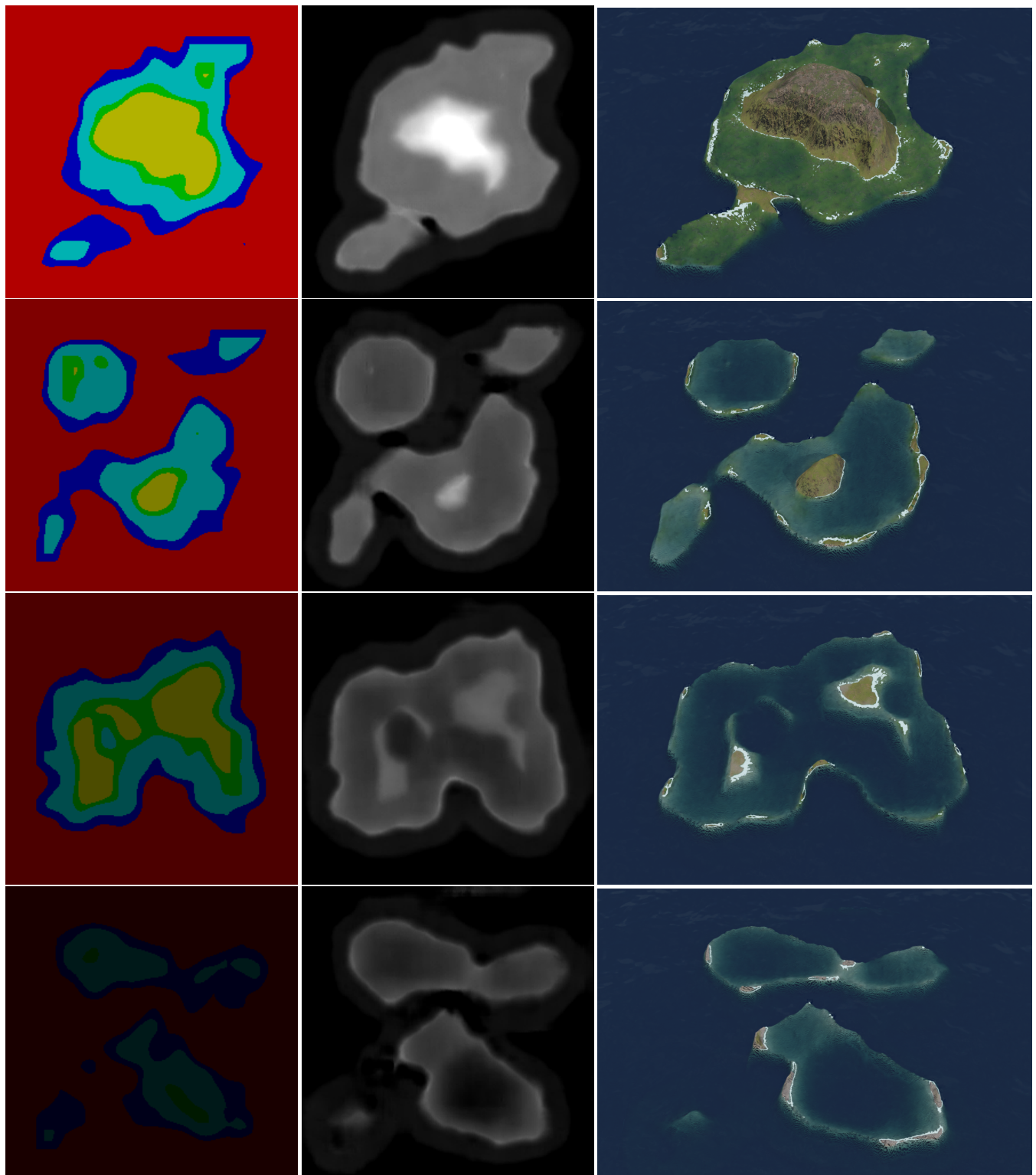


**Figure 16:** Starting from random Perlin noise, transformed into label maps with increasing subsidence, we can generate a large variety of results.